

# Fault activity, tectonic segmentation, and deformation pattern of the western Himalaya on Ma timescales inferred from landscape morphology

Markus Nennowitz, Rasmus C. Thiede\*, and Bodo Bookhagen

UNIVERSITY OF POTSDAM, INSTITUTE FOR EARTH AND ENVIRONMENTAL SCIENCE, KARL-LIEBKNECHT-STR. 24-25, 14476 POTSDAM, GERMANY

## ABSTRACT

The location and magnitude of Himalayan tectonic activity has been debated for decades, and several aspects remain unknown. For instance, the spatial distribution of crustal shortening that ultimately sustains Himalayan topography and the activity of major fault zones remain unknown at Ma timescales. In this study, we address the spatial deformation pattern in the data-scarce western Himalaya. We calculated catchment averaged, normalized river-steepness indices of non-glaciated drainage basins with tributary catchment areas between 5 and 200 km<sup>2</sup> (n = 2138). We analyzed the spatial distribution of the relative change of river steepness both along and across strike to gain information about the regional distribution of differential uplift pattern and relate this to the activity of distinctive fault segments. For our study area, we observe a positive correlation of averaged  $k_{sn}$  values with long-term exhumation rates derived from previously published thermochronologic datasets combined with thermal modeling as well as with millennial timescale denudation rates based on cosmogenic nuclide dating. Our results indicate three tectono-geomorphic segments with distinctive landscape morphology, structural architecture, and fault geometry along the western Himalaya: Garhwal-Sutlej, Chamba, and Kashmir Himalaya (from east to west). Moreover, our data recognize distinctive fault segments showing varying thrust activity along strike of the Main Frontal Thrust, the Main Boundary Thrust, and in the vicinity of the steep topographic transition between the Lesser and Greater Himalaya. In this region, we relate out-of-sequence deformation along major basement thrust ramps, such as the Munsiri Thrust with deformation along a mid-crustal ramp along the basal décollement. We suggest that during the Quaternary, all major fault zones in the Western Himalaya experienced out-of-sequence faulting and have accommodated some portion of crustal shortening.

LITHOSPHERE

GSA Data Repository Item 2018222

<https://doi.org/10.1130/L681.1>

## INTRODUCTION

Active crustal shortening along major fault zones is responsible for the growth of the Himalaya (Fig. 1). Recent geodetic data sets provide detailed decadal-timescale estimates of the interseismic elastic and distributed shortening across the entire orogen (e.g., Wang et al., 2001; Paul et al., 2001; Banerjee, 2002; Banerjee et al., 2008; Kundu et al., 2014; Stevens and Avouac, 2015). Deformation models and geophysical and geologic data suggest (Fig. 1) that shortening is mainly accommodated by active out-of-sequence deformation along basement thrust ramps (e.g., Wobus et al., 2003; Whipple et al., 2016; Thiede et al., 2017; Stübner et al., 2018) or by slip along a basal décollement including an orogen parallel ramp geometry (e.g., Bilham et al., 1997; Cattin and Avouac, 2000; Meade, 2010; Ader et al., 2012). However, seismic and geodetic measurements only reflect present-day conditions. Empirical data and field verification of shortening rates along the Himalayan front and across major structures during Pleistocene and Holocene times are sparse and do not allow along-strike comparison. Notable exceptions are shortening rates measured in

central Nepal and the eastern Himalaya, where observed GPS velocities match the rates of Holocene fault activity along the deformation front, the Main Frontal Thrust (MFT) (Lavé and Avouac, 2000; Chirouze et al., 2013; Burgess et al., 2012). Total shortening rates of  $21 \pm 1.5$  mm/yr and  $23 \pm 6$  mm/yr, respectively, are accommodated. However, neither the spatial nor temporal resolution of deformation rates allow extrapolation of the central Nepal fault activity to other segments toward the west. Until now, data availability has been insufficient to assess fault geometry and kinematics of the deformation process at the entire mountain front on longer timescales.

Recent studies suggest that shortening and deformation in the Himalaya is not uniformly accommodated: data from geophysical surveys, thermochronologic studies, and balanced cross sections suggest that the Himalayan front is separated in multiple orogenic segments (e.g., Yin, 2006; Robert et al., 2011; Coutand et al., 2014; McQuarrie et al., 2015; van der Beek et al., 2016; Hetényi et al., 2016). For instance, a recent geophysical study proposed to recognize an active basement thrust ramp that is located in the hanging wall of a basal décollement (Caldwell et al. 2013) directly beneath the physiographic transition zone (referred to as PT2 in central Nepal, cf. Wobus et al., 2003). Recent studies based on the spatial pattern of river-steepness indices indicate lateral discontinuities of respective segments in central and western Nepal (Harvey et al., 2015; van der Beek et al., 2016).

Rasmus Thiede  <http://orcid.org/0000-0003-1740-7547>

\*Corresponding author; present address: Christian-Albrechts-University Kiel, Institute for Geosciences, Ludewig-Meyn-Straße 10, 24118 Kiel, Germany

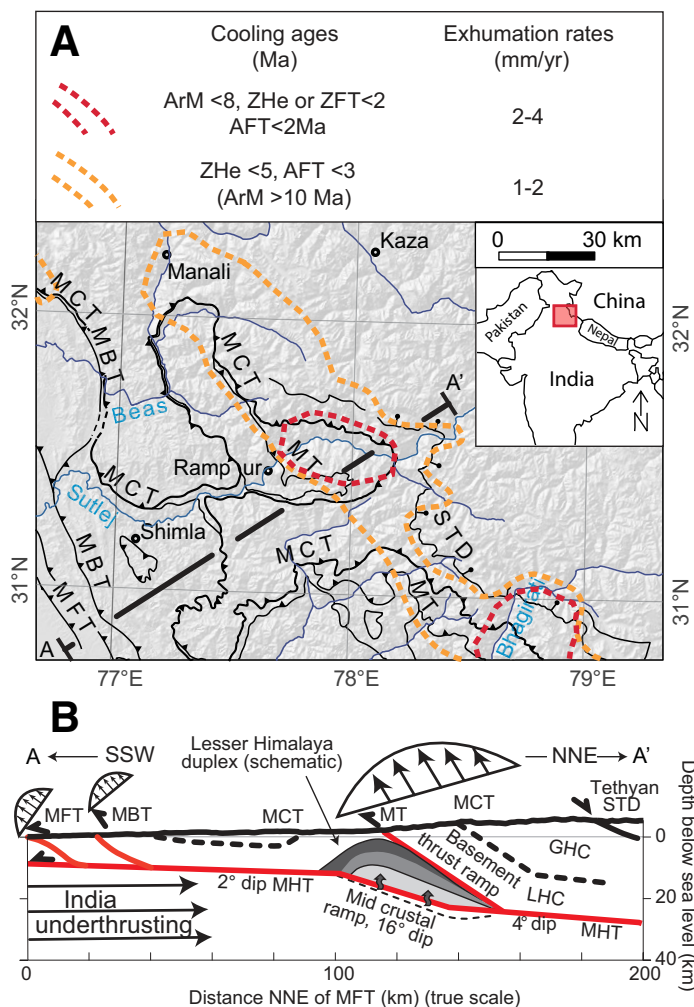


**Figure 1.** Schematic pattern of tectonic deformation and exhumation across the Indian southern Himalayan front since the late Miocene until present day, based on thermochronologic data and thermal modeling (Thiede and Ehlers 2013; Thiede et al., 2017; Stübner et al., 2018): (A) in map view and (B) cross section (modified from Caldwell et al., 2013). Black arrows indicate contribution of overthrusting within the Himalayan wedge (~25% of total shortening) and underthrusting component of India (75%) (Lavé and Avouac, 2001). Profile crossing the Himalaya along the Sutlej Valley (Profile A–A') is representative of the western end of the central Himalaya. Here, the rapid exhumation (1–4 mm/yr) of the high-grade metamorphic core along the southern front of the High Himalaya accommodates about ~50–75% of total overthrusting component. Abbreviations: AFT—apatite fission track; ArM—white mica  $^{40}\text{Ar}/^{39}\text{Ar}$  date; GHC—Greater Himalayan Crystalline; LHC—Lesser Himalayan Crystalline; MBT—Main Boundary Thrust; MCT—Main Central Thrust; MFT—Main Frontal Thrust; MHT—Main Himalayan Thrust; MT—Munsiari Thrust; STD—South Tibetan Detachment System; ZHe—zircon  $^{238}\text{U}$ - $^{232}\text{Th}/^4\text{He}$  dating; ZFT—zircon fission track.

In summary, previous studies suggest an along-strike spatiotemporal inhomogeneity in crustal deformation pattern. In this study, we address the spatial deformation pattern in the western Himalaya. We rely on digital topography to calculate normalized river-steepness indices ( $k_{sn} \theta = 0.45$ ) (e.g., Wobus et al., 2006b; Kirby and Whipple, 2012) for tributary catchments, analyze their spatial structure, and present results with orogen-perpendicular and along-strike swath profiles to identify changes along the

western Himalayan mountain front (Fig. 2A). Longitudinal-river profiles and changes in their steepness can be used as proxies of differential rock uplift for topographic steady-state settings (Seeber and Gornitz, 1983; Howard et al., 1994; Whipple and Tucker, 1999; Kirby and Whipple, 2012). In general, channel profiles of Himalayan rivers draining southward are not well graded and show major deviations from equilibrated ones, which is predicted by the stream power law when a balance of erosion and rock uplift with steady-state topography is established (e.g., Wobus et al., 2006b; Robl et al., 2008; Stüwe et al., 2008). The intention of our study is to identify the lateral extent of structural segments, such as proposed orogen-parallel basement ramp structures, which accommodate shortening and uplift. Our results underline the spatial complexity of both across- and along-strike deformation patterns and improve our understanding of where differential uplift and faulting has been accommodated on  $10^4$ – $10^6$  yr timescales.

**GEOLOGIC SETTING**

Previous research has helped to understand and quantify the formation process of the Himalaya (e.g., Molnar and Tapponier, 1975; England and Molnar, 1997; Hodges, 2000). The majority of deformation was accommodated along major thrust systems that can be traced along-strike of the entire Himalaya (e.g., Gansser, 1964; Steck et al., 2003). During the accretion and subduction process, parts of the sedimentary coverage of the Indian plate were detached during underthrusting of the Himalayan wedge, underwent different degrees of regional metamorphism, and accreted to the base of the wedge (Bollinger et al., 2006) forming the Lesser Himalayan duplex (LH-duplex) (DeCelles et al., 2001; Robinson et al., 2003). This ultimately resulted in the lithologic units of the Lesser (LH) and Greater Himalaya (GH). The continuing convergence during Early and Mid-Miocene led to the formation of the Main Central Thrust (MCT), which placed GH high-grade metamorphic units atop low-grade metasediments of the LH. During the late Miocene, the deformation had migrated southward and the predominantly pre-tertiary units of the LH were thrust over the foreland molasse by north dipping faults of the Main Boundary Thrust Zone (MBT) (Meigs et al., 1995; Thiede et al., 2017). In the Kashmir Himalaya to the west, the large intramontane Kashmir Basin formed when the locus of thrusting and uplift transferred from the northern to the southern margin of the basin between 4 and 1 Ma (Burbank, 1983; Burbank and Johnson 1983). The Pir Panjal Range resulted from enhanced activity along the MBT, uplifting the southern margin of the basin. Prior to 1.7 Ma, the Medicott-Wadia Thrust (MWT) evolved as a southern splay fault of the MBT (Thakur et al., 2010; Gavillot et al., 2016). As the product of Miocene Himalayan erosion, the Siwalik units were deposited as the foreland molasse (Powers et al., 1998). Due to the growth and propagation of the orogenic wedge during the Quaternary, the Siwalik Molasse has been deformed and uplifted by a forward propagating sequence of brittle faults, of which the MFT is the youngest one bounding the Sub-Himalaya to the south (e.g., Thakur et al., 2007). Although of variable distance to each other, the three major fault zones, MCT, MBT, and MFT, are exposed along the entire length of the Himalayan orogen and merge at depth into a joint décollement, the Main Himalayan Thrust (MHT) (e.g., Seeber and Armbruster, 1981; Nábelek et al., 2009).

Researchers have been arguing for decades about the geometry of the MHT, the existence of out-of-sequence thrusts, and their contribution to Himalayan crustal shortening (e.g., Bollinger et al., 2006; Lavé and Avouac, 2000; Wobus et al., 2006a; Whipple et al., 2016; Elliott et al., 2016; van der Beek et al., 2016). It has been argued that a pronounced crustal ramp structure in the basal décollement plays an important role for

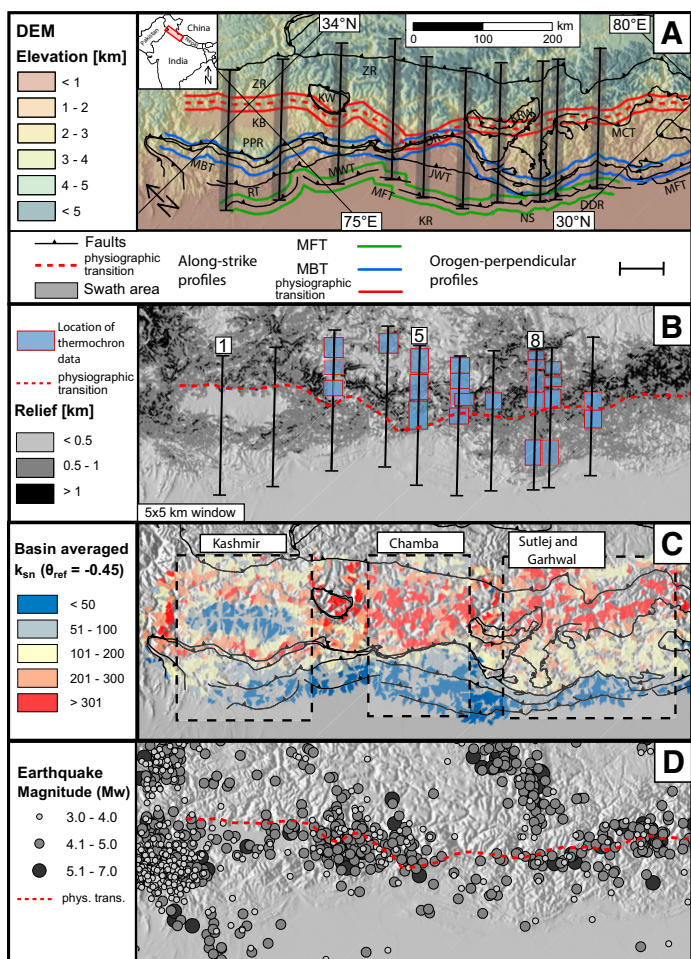


**Figure 2.** (A) Topographic map and swath profile locations. Colored lines show location of traces of along-strike swath profiles. Lines in the hanging and footwall are 10 km off the respective structure. Swath profiles (20 km wide) have been calculated along these lines. Black lines show the location of topographic swath profiles (profiles are numbered 1–10 from NW to SE). The locations of the MFT and the MBT were derived from geologic maps by Steck et al. (2003). Abbreviations: DDR—Dehra Dun reentrant; DR—Dhauladhar Range; JWT—Jawalumukhi Thrust; KB—Kashmir Basin; KR—Kangra reentrant; KRW—Kullu-Rampur Window; KW—Kishtwar Window; MBT—Main Boundary Thrust; MCT—Main Central Thrust; MFT—Main Frontal Thrust; MWT—Medicott-Wadia Thrust; NS—Nahan Salient; PPR—Pir Panjal Range; RT—Riasi Thrust; ZR—Zaskar Range. (B) Topographic relief calculated over a 5 × 5 km window. PT2 is defined by the abrupt increase in topographic relief (relief > 1000 m). Thermochronologic data and erosion rates are obtained from Thiede et al. (2009, 2017), Deeken et al. (2011), and Thiede and Ehlers (2013). (C) Spatial pattern of catchment-averaged river steepness analysis for the western Himalaya with  $\theta_{ref} = -0.45$ . The three segments, Kashmir Himalaya, Chamba Himalaya, and Garhwal-Sutlej Himalaya are areas of internally similar morphologic, geologic, and topographic characteristics. (D) Distribution of moment magnitudes (Mw) of seismic events since 1960 (data source: U.S. Geological Survey, <http://earthquake.usgs.gov/earthquakes/search>).

building topography, forming the major physiographic transition (PT2), and defining the location by imposing a strong gradient in exhumation patterns during growth of the LH duplex (e.g., Schelling and Arita, 1991; Pandey et al., 1995; Lavé and Avouac, 2000; Herman et al., 2010; Robert et al., 2011). Alternative studies have favored the idea that the MHT flat

must extend farther north than the position of the ramp hypothesized to explain the PT2 (Whipple et al., 2016; Wobus et al., 2006a). In central Nepal the PT2 is characterized by rapid elevation and relief increase accompanied with highly steepened river channels that have been documented from the central Himalaya to the Sutlej/Beas region in the west (Seeber and Gornitz 1983; Wobus et al., 2003). In the western central Himalaya, increasing evidence supports the existence of a steep basement thrust ramp in the hanging wall of a LH-duplex (Stübner et al., 2018), and its surface exposure has been related to the Munsiri Thrust (MT) (Cadwell et al., 2013). Recent studies imply that this structure is active and has rapidly exhumed late Miocene-Pliocene high-grade metamorphic rocks from mid-crustal levels to the surface since 7–8 Ma (Vannay et al., 2004; Stübner et al., 2018). Pressure-temperature-time data indicate that the MT and MCT hanging wall rocks represent distinct tectonic units of the metamorphic core with different origins and were decoupled during their Miocene extrusion (Vannay et al., 2004; Caddick et al., 2007; Thöni et al., 2012).

**METHODS**

The stream power law relates the slope (S) along a longitudinal river profile as a power-law function of upstream area (A), the normalized steepness index ( $k_{sn}$ ), and the concavity index ( $\theta_{ref}$ ) (Flint, 1974; Whipple and Tucker, 1999):

$$S = k_{sn} A^{-\theta_{ref}} \tag{1}$$

Changes in the river’s base level will lead to a change in the erosion rate, resulting in the adjustment of the longitudinal profile by headward migration of a knickpoint. Thus, under the assumption of uniform bedrock strength and uniform runoff, investigating the spatial distribution of river steepness indices can provide a relative measure for identifying active deforming and uplifting domains across mountain belts.

We use the TopoToolbox (<https://github.com/wschwanghart/topotoolbox>) (Schwanghart and Scherler, 2014) and an automated river profile analyzer (Neely et al., 2017). Our analysis is based on the SRTM-1 dataset (NASA JPL, 2013) with a nominal spatial resolution of 30 m.

We calculate  $k_{sn}$  indices for channel segments of tributaries with a reference concavity of  $\theta_{ref} = -0.45$  to maintain the comparability of river segments with highly varying upstream areas. The obtained results are averaged for catchments with a Strahler-stream order of 3, resulting in drainage areas between 5 and 250 km<sup>2</sup>.

We exclude drainage basins dominated by glacial erosion from the analysis, because they have inherited profiles that differ from those eroded by fluvial processes (Brocklehurst and Whipple, 2007). We mapped terminal moraines from satellite images and used their upstream areas as masks to exclude glacially dominated areas from the obtained stream dataset. Drainage basins characterized by both fluvial and glacial erosion are included and have been assigned the average  $k_{sn}$  index of the residual fluvial channel. Moderate transient river-profile features have been observed, but these are similar in nature along strike and do not bias steepness indices (Robl et al., 2017).

Furthermore, we analyzed the elevation data for ten 20-km-wide and 200-km-long orogen perpendicular swath profiles across the western Himalaya (see Fig. 2A for profile locations). Additional and similar swath profiles were obtained strike-parallel and run in the hanging and footwall of the MFT, MBT, and the topographic transition of the MT and MCT. In order to minimize local effects, we display the strike-parallel values averaged for 10-km-wide bins. In addition, two strike parallel swath profiles have been analyzed with 10- and 30-km distances into

the hanging wall of major fault zones (Data Repository Figs. S9 and S10<sup>1</sup>) and their difference (Data Repository Fig. S11).

**RESULTS: DIGITAL TOPOGRAPHIC ANALYSIS OF THE WESTERN HIMALAYA**

The spatial distribution of averaged catchment steepness indices shows low values (<80 m<sup>0.9</sup>) in the Sub-Himalaya that rapidly increase when crossing the MBT (<100– >200 m<sup>0.9</sup>) and the topographic transition (>300–600 m<sup>0.9</sup>) to the NE. But the magnitude of the  $k_{sn}$  values and their spatial distribution differ along strike of the Himalaya (Fig. 2C). In order to quantify this difference, we have (1) analyzed ten NE-SW orogen-perpendicular 20-km-wide swath profiles (Fig. 2A; see profile 1, 5 and 8 in Fig. 2B for swath-profile location) and (2) eight along-strike swath profiles in the hanging and the footwall of the fault traces of the MFT, the MBT, and the topographic transition (see Fig. 2A for swath-profile location; hanging wall profiles are in Data Repository Figs. S2–S8).

Our averaged  $k_{sn}$  values correlate with estimated exhumation rates obtained by 1D and 2D-thermal models (Fig. 3) (Thiede et al., 2009; Thiede and Ehlers, 2013; Thiede et al., 2017; Stübner et al., 2018). Also, respective values fall in the same range as previously published  $k_{sn}$  values (Scherler et al., 2014; Olen et al., 2016; van der Beek et al., 2016) and denudation rate correlations observed in the Yamuna and Ganges catchment (Fig. 2C).

**NE-SW-Orogen-Perpendicular Profiles**

We first present three characteristic orogen-perpendicular profiles with representative changes (additional profiles are shown in the Data Repository item). The three profiles show distinctive elevation and channel steepness patterns that allow us to divide the study area into three tectono-morphic units that we call Kashmir, Chamba, and Garhwal-Sutlej Himalaya (Fig. 4).

**Kashmir Himalaya**

The most characteristic topographic feature of the Kashmir Himalaya is the intramontane Kashmir Basin between the Pir Panjal and the Zaskar Ranges (c.f. Fig. 2A for location). It is located at a mean elevation of 1600 m with northeast-dipping Tethyan and GH units on both basin margins and has low relief and gentle river channels. The  $k_{sn}$  indices of the Sub-Himalaya in the Kashmir Himalaya increase smoothly toward the Pir Panjal Range, including minor peaks in the hanging wall of the MFT and the MWT. Steepness values in the hanging wall of the MBT profiles rise rapidly to plateau level ( $k_{sn} > 300 \text{ m}^{0.9}$ ) and correlate with the topographic expressions of the Pir Panjal and the Zaskar Ranges (Fig. 4A). Further northward, the channel steepness decreases ( $k_{sn} < 200 \text{ m}^{0.9}$ ).

**Chamba Himalaya**

This segment is characterized by a very sharp topographic transition north of the Sub-Himalaya. Along this pronounced mountain front formed by the MBT hanging wall, we observe the highest values in the catchment-averaged channel steepness index for this segment (>350 m<sup>0.9</sup>). In the frontal fold-and-thrust belt of the Sub-Himalaya, catchments show

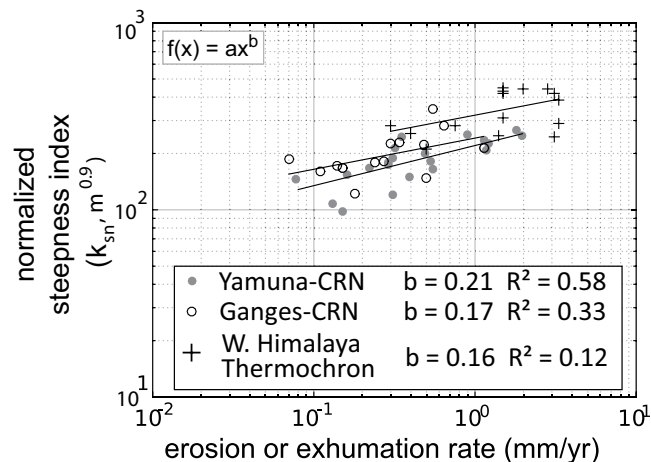


**Figure 3. Correlation between millennial-timescale erosion rates derived from cosmogenic radionuclide measurements (Olen et al., 2016; Scherler et al., 2014) and Ma-timescale exhumation rates derived from thermochronologic data combined with thermal modeling (Thiede et al., 2009; Thiede and Ehlers, 2013; Thiede et al., 2017; Stübner et al., 2018) and catchment-averaged steepness indices. Despite differences in timescales, we observe a positive correlation between averaged normalized steepness indices and modeled exhumation denudation rates.  $k_{sn}$ —normalized steepness index;  $m$ —reference concavity;  $b$ ,  $a$ ,  $x$ —variables in the regression function  $f(x)$ ;  $R^2$ —root mean square error; CRN—Cosmogenic radio nuclide data.**

minor increases in the steepness indices in the vicinity of the Jwalamukhi thrust (Fig. 4B). Moving northeast along the profile, the values decrease as observed within the Kashmir Himalaya ( $k_{sn} < 200 \text{ m}^{0.9}$ ).

**Garhwal-Sutlej Himalaya**

The topographic characteristics typical for the Garhwal-Sutlej segment are comparable to the characteristics of central Nepal (Wobus et al., 2006a). In contrast to the Kashmir and the Chamba segments, we notice a stepwise increase in the elevation and in the  $k_{sn}$  indices in the hanging wall of the MBT and the topographic transition (profiles 8–10), respectively (Fig. 4C).

**NW-SE-Along-Strike Profiles**

In a profile along the topographic transition (Figs. 2A and 5A), we observe variation in the difference of averaged  $k_{sn}$  indices between catchments located in the hanging and in the footwall. Maximum differences are located at the Zaskar Range (north of the Kashmir Basin), at the Kishtwar Window, the Dhauladhar Range, and with a southeastward increasing trend in the Garhwal-Sutlej Himalaya (Fig. 5A). There is a large lithologic contrast along the northern Kashmir Basin margin and Dhauladhar Range between depositional alluvium in the footwall and erosional topography of crystalline rocks in the hanging wall. However, these do not explain the convex shape within the segment, where maximum differences are in the center and decrease toward the margins. Along strike of the MBT

<sup>1</sup>GSA Data Repository Item 2018222: Supplementary Figure S1 schematically shows the structural setting at the Himalayan front in the Garhwal, Sutlej, Chamba, and Kashmir region. Supplementary Figures S2–S8 show orogen-perpendicular swath profiles used in our study, except profiles 1, 5, and 8, which are presented in Figure 3 (cf. Figure 1A for location). The remaining 7 profiles show elevation data, catchment-averaged river-steepness indices, and exhumation rates in the swath area. Supplementary Figures S9 and S10 show the along-strike changes in  $k_{sn}$  in the hanging wall of the major structures, MFT, MBT, and the physiographic transition. Profile values in Supplementary Figure S9 are averaged catchment values 10 km offset of the structures. Profile values in Supplementary Figure S10 are similarly gained, 30 km offset of the respective structure. Supplementary Figure S11 presents the difference between  $k_{sn}$  indices 30 km and 10 km in the hanging wall of the structures. The data repository item is available at <http://www.geosociety.org/datarepository/2018>, or on request from [editing@geosociety.org](mailto:editing@geosociety.org).

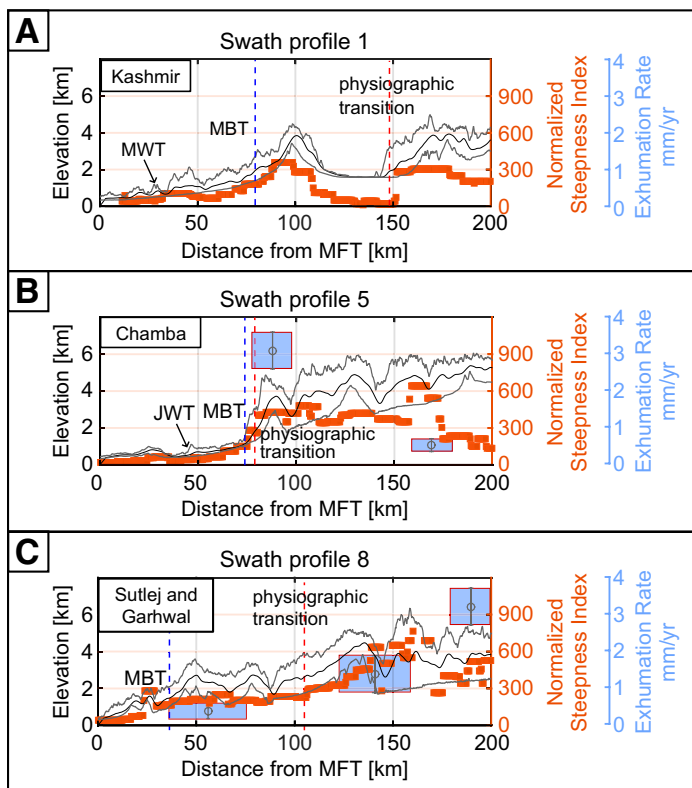


**Figure 4.** Swath profiles representing the topographic characteristics for the Kashmir, Chamba, and Garhwal-Sutlej Himalaya. Black lines indicate mean elevation, and gray lines show minimum/maximum elevation. Orange boxes are mean values for catchment-averaged steepness indices (cf. Fig. 2C). Gray boxes show the modeled exhumation rate for the area (box width), including the standard deviation (box height). The blue dashed lines mark the location of the MBT, and the red lines show the physiographic transition in the profile. The distribution of the topometric parameters suggests a tectonic segmentation of the western Himalaya. JWT—Jawalumukhi Thrust; MWT—Medicott-Wadia Thrust.

(Figs. 2A and 5B), we recognize three distinct and separate fault segments, which show large differences in the averaged steepness indices across the fault. These along-strike variations have an arched distribution in the  $k_{sn}$ -difference patterns, and we propose that this is analogous to the slip distribution along faults. 150–200-km long segments can be assigned to faults segments in the MBT west of the Chenab outlet, the Dhauladhar Range, and the northern boundary of the Dehra Dun reentrant.

At the MFT (green profile in Figs. 2A and 5C), the catchments show little differences between the hanging wall and the footwall, and their steepness indices are generally low. Catchments characterized by increased  $k_{sn}$  indices in the hanging wall are related to segments, within the narrow Sub-Himalaya, where faulting is mostly localized in the hanging wall of the MFT (Fig. 2C).

**DISCUSSION**

**Caveats and Limits to the Analysis**

The  $k_{sn}$  index is not only sensitive to variations in tectonic rock uplift, but may also be biased by differences in erosive resistivity across lithological and geological boundaries, precipitation gradients, presence of

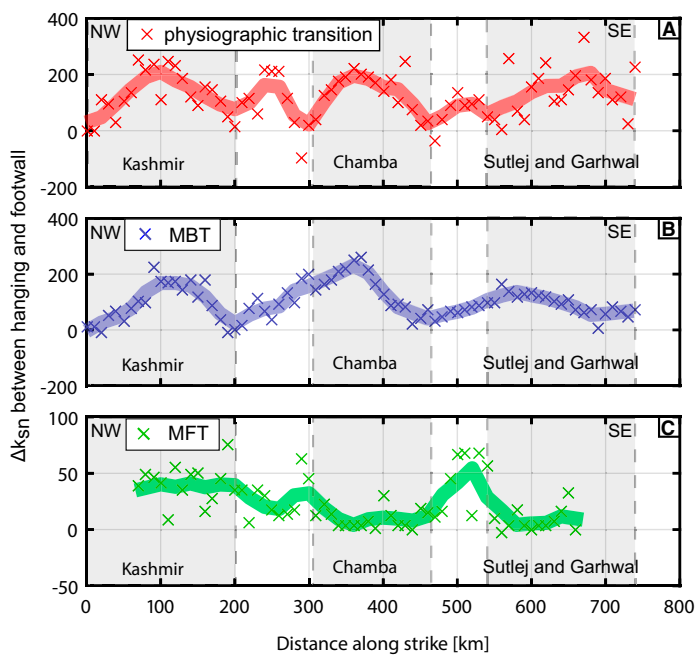


**Figure 5.** Differences of  $k_{sn}$  values between catchments in the hanging and footwall along strike of the three major fault zones with a shaded area indicating a 50-km running average. See Figure 2A for location. Crosses show  $\Delta$  river steepness indices between hanging and footwall averaged over 10-km segments (note different y-scales). Areas of an increased difference in steepness indices are interpreted to show fault segments with Quaternary tectonic activity. (A) The contribution of the PT2-structure to higher steepness indices in its hanging wall is pronounced at the northern boundary of the Kashmir Basin (50–150 km), at the Dhauladhar Range (340–410 km) and in the Garhwal-Sutlej Himalaya (600–800 km). (B) The MBT profile shows three parabola-like increases at the Pir Panjal Range (50–150 km), at the Dhauladhar Range (300–400 km), and in the northern boundary of the Dehra Dun (540–640 km). (C) The MFT profile shows a large positive  $\Delta k_{sn}$  between Chamba and Sutlej regions (460–540 km), around the Chenab outlet (280–320 km), and in the Kashmir Himalaya (60–220 km). See the Data Repository Item (text footnote 1) for additional along strike  $k_{sn}$  plots showing changes in the hanging wall (10 and 30 km) of the major fault systems (Data Repository Figs. S9–S11).

glaciated areas, and the influences of valley fill and temporary alluvial cover of otherwise bedrock rivers (Kirby und Whipple 2012; Bookhagen and Strecker, 2012). Our analysis covers the spatial distribution of  $k_{sn}$  values on a sub-orogenic scale. In the following, we assess the influence of biasing factors.

While the main lithologic units remain similar along strike of the Himalayan orogen (e.g., Hodges, 2000; Yin, 2006), there exist differences in rock strength and deformation history that may explain some of the observed scatter in strike-parallel profiles. However, we argue that lithologic changes are negligible for the main trend in these profile analyses of the  $k_{sn}$  indices (Scherler et al., 2014; Olen et al., 2016).

From a climatic and environmental perspective, there is little evidence for steep E-W climatic and vegetation-cover gradients that may explain along- or across-strike variations in channel steepness (Scherler et al., 2014; Olen et al., 2016; van der Beek et al., 2016; Scherler et al., 2017). For example, annual precipitation data show only low along-strike changes, but a very pronounced N-S gradient, which is highest around the topographic transition (Bookhagen and Burbank, 2010). The associated high discharge leads to an increase in the erosional efficiency and thus to

a decrease in the river steepness, as also shown in other areas (Bookhagen and Strecker, 2012). Similarly, vegetation cover exhibits along-strike variations, but these are low at the scale of this study (Olen et al., 2016).

Alluvial rivers are common in the Sub-Himalaya and within the Kashmir Basin with incision processes and rates other than those observed in bedrock rivers. Most rivers in the LH and GH are bedrock rivers in which sediment-covering river channels moved at least during catastrophic discharge events (e.g., Wulf et al., 2010; Scherler et al., 2014). These systematic changes of river characteristics possibly explain parts of the large orogen-perpendicular  $k_{sn}$ -gradients observed between the Sub-Himalaya and LH (cf. Fig. 3 at the MBT) and are more important than lithologic strength variations between these units. In summary, changes between alluvial and bedrock rivers are mainly limited to the physiographic units and do not explain variation observed along-strike in the western Himalaya.

### Relation of Channel Steepness and Rock Uplift in the Western Himalaya

Exhumation rates derived from low-temperature thermochronology and thermal modeling for the study region range between  $<0.5$  and  $\sim 4$  mm/yr on Ma timescales (Thiede and Ehlers, 2013; Thiede et al., 2017; Stübner et al., 2018). It has been shown that channel steepness indices are useful proxies for recognizing spatial distribution of differential uplift across entire orogenic fronts (e.g., Kirby and Whipple, 2001; Bookhagen and Strecker, 2012; Scherler et al., 2015; Olen et al., 2015). Our data suggest a positive correlation between catchment-averaged, normalized steepness indices and the regional exhumation rate (Fig. 3). Unfortunately, underlying thermochronologic data distribution is often too sparse and correlation with normalized steepness indices too weak to interpolate the calculated exhumation rates across the entire western Himalaya. However, the positive correlation supports the relation between channel steepness indices and exhumation rates ranging on timescales between 0 and 4 Ma.

### Topographic Development and Relation to Decadal-Timescale Shortening Rates

Geodetically measured shortening rates agree well with long-term models of Indian north convergence, with a rotation pole west of India (Molnar and Stock, 2009): these are  $12 \pm 1$  mm/yr for the Kashmir Himalaya (Kundu et al., 2014),  $14 \pm 1$  mm/yr for the Chamba Himalaya (Banerjee, 2002), and  $19 \pm 1$  mm/yr for the Garhwal-Sutlej Himalaya (Stevens and Avouac, 2015). This suggests a consistent shortening rate since at least the Quaternary, if not longer.

Multiple studies propose that a large portion of the arc perpendicular strain is accommodated by slip along the MHT, as well as internal shortening or a combination of internal uplift and frontal accretion (Powers et al., 1998; Wesnousky et al., 1999; Thakur et al., 2014; Gavillot et al., 2016; Thiede et al., 2017).

Based on the distribution of  $k_{sn}$ , exposed geologic units, and regional distribution of major fault systems, we propose that the western Himalayan topography is formed by three independent deforming segments. Each segment accommodates shortening along different fault splays, fault kinematics, and fault geometries.

We hypothesize that the three segments were tectonically decoupled from each other during the Quaternary or longer times. We conclude that the growth of topography is not limited exclusively to shortening accommodated along the MFT and movement along the MHT mid-crustal ramp in the western Himalaya, as is proposed for parts of the central Himalaya (Lavé and Avouac, 2001). Instead, we suggest that a combination of coeval frontal and internal deformation along multiple fault systems,

such as out-of-sequence faults within the Sub-Himalaya (e.g., Jwalamukhi and Riasi fault systems; cf. Fig. 2A; Gavillot et al., 2016), MBT activity (Thiede et al., 2017), and displacement along major basement thrust ramps like the MT combined with a MHT-ramp in the Sutlej (Vannay et al., 2004; Stübner et al., 2018) and Garhwal segment (Data Repository Fig. S1), has accommodated Quaternary shortening.

### Spatiotemporal Patterns of Deformation in the Western Himalaya

By comparing topographic swath profiles and channel steepness indices across the western Himalaya, we recognize major changes in the vicinity of primary fault systems such as the MT, MBT, and MFT (Fig. 4). We observe varying differences in the river-steepness indices between hanging and footwall catchments (Fig. 5), which indicates recent differential rock uplift across these zones. This is supported by previous findings by Seeber and Gornitz (1983) and Wobus et al. (2003, 2006) for central Nepal. Interestingly, this indicates that the main fault systems still contribute to the deformation and uplift of the wedge, for example through active basement thrust ramps, but that this contribution is not uniform along strike of the western Himalaya (Fig. 2). Below, we highlight the three main patterns and their implication from north to south.

First, topographic steepness changes across either the topographic transition between the LH and GH or documented basement thrust ramps in the Dhauladhar Range (MBT), Garhwal-Sutlej Himalaya (MT) (Data Repository Fig. S1) suggest that at least some part of the shortening has been accommodated by out-of-sequence thrusting during the Quaternary. Combining recently published geophysical data and thermochronologic studies of these regions indicate the existence of a basement thrust ramp along the northern roof of the Lesser Himalayan Duplex (Caldwell et al., 2013; Stübner et al., 2018). Furthermore, this is supported by studies documenting that the metamorphic core exposed in the Sutlej Valley and Garhwal comprises both LH- and GH-rocks with documented discrete exhumation paths (Vannay et al., 2004; Caddick et al., 2007; Célérier et al., 2009; Thöni et al., 2012). After apparent diminution of the MCT fault system in the middle Miocene (prior to 10 Ma), late Miocene peak metamorphism requires rapid continuous exhumation of the MT hanging wall since  $\sim 8$  Ma until present (Vannay et al. 2004; Stübner et al., 2018, and references therein) and therefore implies that the MT forms an active basement thrust ramp. In summary, we argue for a combined exhumation across a MHT mid-crustal ramp and a MT-basement thrust ramp in the Sutlej and Garhwal segment.

Further west, both the northeastern and southwestern Kashmir Basin margins are characterized by major northeast-dipping thrust complexes (Burbank, 1983) and by increased  $k_{sn}$  values. Faulting along the northeastern Kashmir margin has diminished since 0.5–1 Myr ago (Burbank and Johnson, 1983), but river profiles have not been equilibrated since then (Fig. 4A).

Second, along-strike variations of channel steepness indices at the MBT suggest major fault activity and segmentation. Using digital topography, we were able to recognize tectonically active segments. Topography in the hanging wall segments west of the Chenab outlet (Gavillot et al., 2016, and references therein), at the Dhauladhar Range (Thiede et al., 2017), and at the northern boundary of the Dehra Dun reentrant (c.f. Fig. 2A for location) have been uplifted due to faulting of the respective MBT-fault segments. For some of those, Quaternary fault activity has been previously proposed (Yeats and Lillie, 1991), but identifying associated geomorphic and paleoseismologic evidences as in western Nepal (Hossler et al., 2016) has been challenging. Based on thermochronologic implications and modeling, we suggest that the MBT forms an active basement

thrust ramp in the Chamba Himalaya (Fig. 2C), and controls the observed increase in topography and relief (Deeken et al., 2011; Thiede et al. 2017).

Third, minor along-strike changes in the hanging wall of the MFT indicate along-strike variation in the fault displacement during the Quaternary. In the Kashmir Himalaya as well as to the southeast in the Nahan Salient (cf. Fig. 2A for location), we identified significant changes in the normalized steepness indices between the hanging and footwalls, indicating a pronounced MFT-fault displacement within these segments during Quaternary time. Paleoseismologic studies argue that the entire length of the MFT has been ruptured during large earthquakes over the last millennium (e.g., Wesnousky et al., 1999; Kumar et al., 2006). Other studies have shown that out-of-sequence faulting within the Sub-Himalaya, as well as rock uplift at the MFT, has been present for the Holocene (Wesnousky et al., 1999; Lavé and Avouac, 2000; Dey et al., 2016; Gavillot et al., 2016; Thakur et al., 2014). Mean Holocene fault displacement rates of  $6.5 \pm 0.5$  mm/yr and  $7 \pm 2$  mm/yr have been published for internal Sub-Himalayan deformation at the Medicott-Wadia Thrust and the Jwalamukhi thrust (Thakur et al., 2010; Gavillot et al., 2016; Dey et al., 2016). However, we only observe minor increases in  $k_{sn}$  values in the hanging wall segments of these faults. These are likely related to lower rock strengths and less consolidated lithologies enabling very high erosion rates of the Sub-Himalaya strata. More importantly the mainly sediment-covered, alluvial river beds dilute changes of  $k_{sn}$  values compared to bedrock rivers that may have otherwise recorded deformation histories within this frontal part of the orogeny.

### Implications for Shortening and Uplift Patterns

The along-strike differences of the  $k_{sn}$  values indicate that the respective active MBT fault segments have a length of  $\sim 150$  km and maximal differences in the center and decrease toward the margins (Fig. 5). Swath profiles in the hanging wall running along strike for 10 and 30 km from major structures show systematic changes of mean  $k_{sn}$  values at segment boundaries (see Data Repository Figs. S9–S10). Along the MT, we observe similar patterns on a smaller length scale ranging between 100 and 150 km. We argue that the observed  $k_{sn}$  differences between the hanging wall and footwall are related to active deformation in the vicinity of major fault zones and correlate with exhumation patterns on Ma timescales (Fig. 2). These differences correlate with a fault displacement pattern with maximal differential uplift in the center and decreases toward the sides, resulting in lower difference values at the periphery of the segment along its transfer zones (Fig. 5). If true, shortening has been accommodated by individual, but large-scale fault segments along strike, using multiple, coevally active out-of-sequence basement thrust ramps across the wedge on millennial- to million-year timescales, and shortening is not limited to deformation along the MHT and MFT. We argue that this deformation regime evolves toward a steady-state topography as predicted by the critical wedge theory (Davis et al., 1983; Dahlen, 1990). We also argue that the observed internal deformation is a combination of the following three factors: (1) thrusting over a crustal ramp of the MHT; (2) deformation along steep basement thrust ramps such as the MT in the Garhwal-Sutlej segment (Caldwell et al., 2013; Negi et al., 2017; Stübner et al., 2018) and a MBT-thrust ramp in the Chamba segment (Thiede et al., 2017); and (3) active thrust ramps along the northern and southern margin of the Kashmir basin during the Quaternary (Burbank and Johnson, 1983).

### CONCLUSION

Based on analysis of the digital topography and synthesis of existing thermochronologic datasets for the western Himalaya, we make the following three key observations.

First, we suggest that the western Himalaya can be separated into three orogenic segments with distinctive morphologic, topographic, geological, and fault-geometrical characteristics. From northwest to southeast, these segments are the Kashmir, Chamba, and Garhwal-Sutlej Himalaya. Our observations are based on the distribution of averaged, normalized steepness indices of tributary catchments. Orogen-perpendicular profiles document that the most pronounced changes of the catchment averaged  $k_{sn}$  values are observed in the vicinity of primary Himalayan fault systems (MFT, MBT, and basement thrust faults such as the MT combined with deformation along a mid-crustal ramp along the MHT).

Second, our data indicate that on Quaternary (if not longer) time-scales, various large-scale fault segments have been independently active across and along the western Himalayan wedge and therefore contribute, although in minor ways, to crustal shortening and impact tectonic uplift patterns. These findings are based on the along-strike differences between the hanging wall and footwall  $k_{sn}$  values of the primary Himalayan fault systems (Fig. 5).

Third, we observe a general positive correlation of catchment-averaged, normalized steepness indices and exhumation rates (where exhumation rates are high) derived from regional thermochronologic datasets for the past 0–4 Ma. Our  $k_{sn}$  values also correlate with catchment-wide denudation rates obtained from published cosmogenic nuclide dating. As shown elsewhere (Kirby und Whipple, 2012; Bookhagen and Strecker, 2012), we argue that first-order normalized steepness indices in the western Himalaya can be used as proxy for detecting differential uplift on a millennial- to million-year timescale. This implies that primary fault zones in the Himalaya are still active and have accommodated rock uplift as well as some portion of crustal shortening on Quaternary or longer timescales.

### ACKNOWLEDGMENTS

We are grateful for the long-standing collaboration and logistical support provided by V. Jain and his group (IIT Gandhinagar, Ahmadabad). Kelin Whipple and two anonymous reviewers are thanked for their contribution to improving this manuscript, and we also thank K. Stüwe for editorial handling. This study was funded by Deutsche Forschungsgemeinschaft (DFG) grants to Thiede (TH 1371/5–1), and Bookhagen acknowledges support from the Ministry of Science and Culture (MWFK) of Brandenburg.

### REFERENCES CITED

- Ader, T., Avouac, J.P., Liu-Zeng, J., Lyon-Caen, H., Bollinger, L., and Galetzka, J., 2012, Convergence rate across the Nepal Himalaya and interseismic coupling on the Main Himalayan Thrust: Implications for seismic hazard: *Journal of Geophysical Research*, v. 117, B04403, <https://doi.org/10.1029/2011JB009071>.
- Banerjee, P., and Bürgmann, R., 2002, Convergence across the northwest Himalaya from GPS measurements: *Geophysical Research Letters*, v. 29, no. 13, p. 30-01–30-04, <https://doi.org/10.1029/2002GL015184>.
- Banerjee, P., Bürgmann, R., Nagarajan, B., and Apel, E., 2008, Intraplate deformation of the Indian subcontinent: *Geophysical Research Letters*, v. 35, no. 18, L18301, <https://doi.org/10.1029/2008GL035468>.
- Bilham, R., Larson, K., and Freymueller, J., 1997, GPS measurements of present-day convergence across the Nepal Himalaya: *Nature*, v. 386, p. 61–64, <https://doi.org/10.1038/386061a0>.
- Bollinger, L., Henry, P., and Avouac, J.P., 2006, Mountain building in the Nepal Himalaya: Thermal and kinematic model: *Earth and Planetary Science Letters*, v. 244, no. 1–2, p. 58–71, <https://doi.org/10.1016/j.epsl.2006.01.045>.
- Bookhagen, B., and Burbank, D.W., 2010, Toward a complete Himalayan hydrological budget: Spatiotemporal distribution of snowmelt and rainfall and their impact on river discharge: *Journal of Geophysical Research*, v. 115, F03019, <https://doi.org/10.1029/2009JF001426>.
- Bookhagen, B., and Strecker, M.R., 2012, Spatiotemporal trends in erosion rates across a pronounced rainfall gradient: Examples from the southern Central Andes: *Earth and Planetary Science Letters*, v. 327–328, p. 97–110, <https://doi.org/10.1016/j.epsl.2012.02.005>.
- Brocklehurst, S.H., and Whipple, K.X., 2007, Response of glacial landscapes to spatial variations in rock uplift rate: *Journal of Geophysical Research*, v. 112, F02035, <https://doi.org/10.1029/2006JF000667>.
- Burbank, D.W., 1983, The chronology of intermontane-basin development in the northwestern Himalaya and the evolution of the Northwest Syntaxis: *Earth and Planetary Science Letters*, v. 64, p. 77–92, [https://doi.org/10.1016/0012-821X\(83\)90054-7](https://doi.org/10.1016/0012-821X(83)90054-7).
- Burbank, D.W., and Johnson, G.D., 1983, The Late Cenozoic chronologic and stratigraphic development of the Kashmir intermontane basin, northwestern Himalaya: *Palaeogeography, Palaeoclimatology, Palaeoecology*, v. 43, p. 205–235, [https://doi.org/10.1016/0031-0182\(83\)90012-3](https://doi.org/10.1016/0031-0182(83)90012-3).

- Burgess, P.W., Yin, A., Dubey, C.S., Shen, Z., and Kelt, T.K., 2012, Holocene shortening across the Main Frontal Thrust zone in the eastern Himalaya: *Earth and Planetary Science Letters*, v. 357–358, p. 152–167, <https://doi.org/10.1016/j.epsl.2012.09.040>.
- Caddick, M., Bickle, M., Harris, N., Holland, T., Horstwood, M., Parrish, R., and Ahmad, T., 2007, Burial and exhumation history of a Lesser Himalayan schist: Recording the formation of an inverted metamorphic sequence in NW India: *Earth and Planetary Science Letters*, v. 264, no. 3–4, p. 375–390, <https://doi.org/10.1016/j.epsl.2007.09.011>.
- Caldwell, W. B., Klemperer, S.L., Lawrence, J.F., Rai, S.S., and Ashish, 2013, Characterizing the Main Himalayan Thrust in the Garhwal Himalaya, India with receiver function CCP stacking: *Earth and Planetary Science Letters*, v. 367, p. 15–27, <https://doi.org/10.1016/j.epsl.2013.02.009>.
- Cattin, R., and Avouac, J.P., 2000, Modeling mountain building and the seismic cycle in the Himalaya of Nepal: *Journal of Geophysical Research*, v. 105, B6, p. 13389–13407, <https://doi.org/10.1029/2000JB900032>.
- Célérier, J., Harrison, T.M., Beyssac, O., Herman, F., Dunlap, W.J., and Webb, A.A.G., 2009, The Kumaun and Garhwal Lesser Himalaya, India: Part 2. Thermal and deformation histories: *Geological Society of America Bulletin*, v. 121, no. 9–10, p. 1281–1297, <https://doi.org/10.1130/B26343.1>.
- Chirouze, F., Huyghe, P., Van Der Beek, P., Chauvel, C., Chakraborty, T., Dupont-Nivet, G., and Bernet, M., 2013, Tectonics, exhumation, and drainage evolution of the eastern Himalaya since 13 Ma from detrital geochemistry and thermochronology, Kameng River Section, Arunachal Pradesh: *Geological Society of America Bulletin*, v. 125, no. 3–4, p. 523–538, <https://doi.org/10.1130/B30697.1>.
- Coutand, I., Whipp, D.M., Gruijic, D., Bernet, M., Fellin, M.G., Bookhagen, B., Landry, K.R., Ghaley, S.K., and Duncan, C., 2014, Geometry and kinematics of the Main Himalayan Thrust and Neogene crustal exhumation in the Bhutanese Himalaya derived from inversion of multithermochronologic data: *Journal of Geophysical Research, Solid Earth*, v. 119, no. 2, p. 1446–1481, <https://doi.org/10.1002/2013JB010891>.
- Dahlen, F.A., 1990, Critical taper model of fold-and-thrust belts and accretionary wedges: *Annual Review of Earth and Planetary Sciences*, v. 18, p. 55–99, <https://doi.org/10.1146/annurev.ea.18.050190.000415>.
- Davis, D., Suppe, J., and Dahlen, F.A., 1983, Mechanics of fold-and-thrust belts and accretionary wedges: *Journal of Geophysical Research*, v. 88, p. 1153–1172, <https://doi.org/10.1029/JB088iB02p01153>.
- DeCelles, P.G., Robinson, D.M., Quade, J., Ojha, T.P., Garzzone, C.N., Copeland, P., and Upreti, B.N., 2001, Stratigraphy, structure, and tectonic evolution of the Himalayan fold-thrust belt in western Nepal: *Tectonics*, v. 20, p. 487–509.
- Deeken, A., Thiede, R.C., Sobel, E.R., Hourigan, J.K., and Strecker, M.R., 2011, Exhumational variability within the Himalaya of northwest India: *Earth and Planetary Science Letters*, v. 305, no. 1–2, p. 103–114, <https://doi.org/10.1016/j.epsl.2011.02.045>.
- Dey, S., Thiede, R.C., Schildgen, T.F., Wittmann, H., Bookhagen, B., Scherler, D., and Strecker, M.R., 2016, Holocene internal shortening within the northwest Sub-Himalaya: Out-of-sequence faulting of the Jwalamukti Thrust, India: *Tectonics*, v. 35, no. 11, p. 2677–2697, <https://doi.org/10.1002/2015TC004002>.
- Elliott, J.R., Jolivet, R., González, P.J., Avouac, J.-P., Hollingsworth, J., Searle, M.P., and Stevens, V.L., 2016, Himalayan megathrust geometry and relation to topography revealed by the Gorkha earthquake: *Nature Geoscience*, v. 9, p. 174–180, <https://doi.org/10.1038/ngeo2623>.
- England, P., and Molnar, P., 1997, The field of crustal velocity in Asia calculated from Quaternary rates of slip on faults: *Geophysical Journal International*, v. 130, p. 551–582, <https://doi.org/10.1111/j.1365-246X.1997.tb01853.x>.
- Flint, J.J., 1974, Stream gradient as a function of order, magnitude, and discharge: *Water Resources Research*, v. 10, p. 969–973, <https://doi.org/10.1029/WR010i005p0969>.
- Gansser, A., 1964, *Geology of the Himalayas*: John Wiley and Sons Ltd. (Regional Geology Series), 308 p.
- Gavillot, Y., Meigs, A., Yule, D., Heermance, R., Rittenour, T., Madugo, C., and Malik, M., 2016, Shortening rate and Holocene surface rupture on the Riasi fault system in the Kashmir Himalaya: Active thrusting within the Northwest Himalayan orogenic wedge: *Geological Society of America Bulletin*, v. 128, no. 7–8, p. 1070–1094, <https://doi.org/10.1130/B31281.1>.
- Harvey, J.E., Burbank, D.W., and Bookhagen, B., 2015, Along-strike changes in Himalayan thrust geometry: Topographic and tectonic discontinuities in western Nepal: *Lithosphere*, v. 7, no. 5, p. 511–518, <https://doi.org/10.1130/L444.1>.
- Herman, F., Copeland, P., Avouac, J.P., Bollinger, L., Mahéo, G., Le Fort, P., Rai, S., Foster, D., Pêcher, A., Stüwe, K., and Henry, P., 2010, Exhumation, crustal deformation, and thermal structure of the Nepal Himalaya derived from the inversion of thermochronological and thermobarometric data and modeling of the topography: *Journal of Geophysical Research, Solid Earth*, v. 115, B06407, <https://doi.org/10.1029/2008JB006126>.
- Hetényi, G., Cattin, R., Berthet, T., Le Moigne, N., Chopel, J., and Lechmann, S., 2016, Segmentation of the Himalayas as revealed by arc-parallel gravity anomalies: *Scientific Reports*, v. 6, p. 33866, <https://doi.org/10.1038/srep33866>.
- Hodges, K.V., 2000, Tectonics of the Himalaya and southern Tibet from two perspectives: *Geological Society of America Bulletin*, v. 112, no. 3, p. 324–350, [https://doi.org/10.1130/0016-7606\(2000\)112<324:TOTHAS>2.0.CO;2](https://doi.org/10.1130/0016-7606(2000)112<324:TOTHAS>2.0.CO;2).
- Hossler, T., Bollinger, L., Sapkota, S.N., Lavé, J., Gupta, R.M., and Kandel, T.P., 2016, Surface ruptures of large Himalayan earthquakes in Western Nepal: Evidence along a reactivated strand of the Main Boundary Thrust: *Earth and Planetary Science Letters*, v. 434, p. 187–196, <https://doi.org/10.1016/j.epsl.2015.11.042>.
- Howard, A.D., Dietrich, W.E., and Seidl, M.A., 1994, Modeling fluvial erosion on regional to continental scales: *Journal of Geophysical Research*, v. 99, no. B7, p. 13971–13986.
- Kirby, E., and Whipple, K.X., 2001, Quantifying differential rock-uplift rates via stream profile analysis: *Geology*, v. 29, no. 5, p. 415–418, [https://doi.org/10.1130/0091-7613\(2001\)029<0415:QDRURV>2.0.CO;2](https://doi.org/10.1130/0091-7613(2001)029<0415:QDRURV>2.0.CO;2).
- Kirby, E., and Whipple, K.X., 2012, Expression of active tectonics in erosional landscapes: *Journal of Structural Geology*, v. 44, p. 54–75, <https://doi.org/10.1016/j.jsg.2012.07.009>.
- Kumar, S., Wesnousky, S.G., Rockwell, T.K., Briggs, R.W., Thakur, V.C., and Jayangondape-rumal, R., 2006, Paleoseismic evidence of great surface rupture earthquakes along the Indian Himalaya: *Journal of Geophysical Research*, v. 111, B03304, <https://doi.org/10.1029/2004JB003309>.
- Kundu, B., Yadav, R.K., Bali, B.S., Chowdhury, S., and Gahalaut, V.K., 2014, Oblique convergence and slip partitioning in the NW Himalaya: Implications from GPS measurements: *Tectonics*, v. 33, no. 10, p. 2013–2024, <https://doi.org/10.1002/2014TC003633>.
- Lavé, J., and Avouac, J.P., 2000, Active folding of fluvial terraces across the Siwalik Hills, Himalayas of central Nepal: *Journal of Geophysical Research*, v. 105, B3, p. 5735–5770, <https://doi.org/10.1029/1999JB900292>.
- Lavé, J., and Avouac, J.P., 2001, Fluvial incision and tectonic uplift across the Himalayas of central Nepal: *Journal of Geophysical Research*, v. 106, B11, p. 26561–26591, <https://doi.org/10.1029/2001JB000359>.
- McQuarrie, N., and Ehlers, T.A., 2015, Influence of thrust belt geometry and shortening rate on thermochronometer cooling ages: Insights from thermokinematic and erosion modeling of the Bhutan Himalaya: *Tectonics*, v. 34, no. 6, p. 1055–1079.
- Meade, B.J., 2010, The signature of an unbalanced earthquake cycle in Himalayan topography?: *Geology*, v. 38, p. 987–990, <https://doi.org/10.1130/G31439.1>.
- Meigs, A.J., Burbank, D.W., and Beck, R.A., 1995, Middle-late Miocene (>10 Ma) formation of the Main Boundary thrust in the western Himalaya: *Geology*, v. 23, no. 5, p. 423–426, [https://doi.org/10.1130/0091-7613\(1995\)023<0423:MLMMFO>2.3.CO;2](https://doi.org/10.1130/0091-7613(1995)023<0423:MLMMFO>2.3.CO;2).
- Molnar, P., and Stock, J.M., 2009, Slowing of India's convergence with Eurasia since 20 Ma and its implications for Tibetan mantle dynamics: *Tectonics*, v. 28, TC3001, <https://doi.org/10.1029/2008TC002271>.
- Molnar, P., and Tapponier, P., 1975, Cenozoic tectonics of Asia: Effects of a continental collision: *Science*, v. 189, no. 4201, p. 419–426, <https://doi.org/10.1126/science.189.4201.419>.
- Nábélek, J., Hetényi, G., Vergne, J., Sapkota, S., Kafle, B., Jiang, M., Su, H., Chen, J., Huang, B.-S., and the Hi-CLIMB Team, 2009, Underplating in the Himalaya–Tibet collision zone revealed by the Hi-CLIMB experiment: *Science*, v. 325, no. 5946, p. 1371–1374, <https://doi.org/10.1126/science.1167719>.
- NASA JPL, 2013, NASA Shuttle Radar Topography Mission Global 1 arc second V003: SRT-MGL, NASA EOSDIS Land Processes DAAC, <https://doi.org/10.5067/MEASURE/SRTM/SRTMGL1.003>.
- Neely, A.B., Bookhagen, B., and Burbank, D.W., 2017, An automated knickzone selection algorithm (KZ-Picker) to analyze transient landscapes: Calibration and validation: *Journal of Geophysical Research. Earth Surface*, v. 122, p. 1236–1261, <https://doi.org/10.1002/2017JF004250>.
- Negi, S., Paul, A., Cesca, S., Kamal, K., Kriegerowski, M., Perugu, M., and Gupta, S., 2017, Crustal velocity structure and earthquake processes of Garhwal–Kumaun Himalaya: Constraints from regional waveform inversion and array beam modeling: *Tectonophysics*, v. 712, p. 45–63, <https://doi.org/10.1016/j.tecto.2017.05.007>.
- Olen, S.M., Bookhagen, B., Hoffmann, B., Sachse, D., Adhikari, D.P., and Strecker, M.R., 2015, Understanding erosion rates in the Himalayan orogen: A case study from the Arun Valley: *Journal of Geophysical Research. Earth Surface*, v. 120, no. 10, p. 2080–2102, <https://doi.org/10.1002/2014JF003410>.
- Olen, S.M., Bookhagen, B., and Strecker, M.R., 2016, Role of climate and vegetation density in modulating denudation rates in the Himalaya: *Earth and Planetary Science Letters*, v. 445, p. 57–67, <https://doi.org/10.1016/j.epsl.2016.03.047>.
- Pandey, M.R., Tandukar, R.P., Avouac, J.P., Lavé, J., and Massot, J.P., 1995, Interseismic strain accumulation on the Himalayan crustal ramp (Nepal): *Geophysical Research Letters*, v. 22, no. 7, p. 751–754, <https://doi.org/10.1029/94GL02971>.
- Paul, J., Bürgmann, R., Gaur, V.K., Bilham, R., Larson, K.M., and Ananda, M.B., 2001, The motion and active deformation of India: *Geophysical Research Letters*, v. 28, no. 4, p. 647–650, <https://doi.org/10.1029/2000GL011832>.
- Powers, P.M., Lillie, R.J., and Yeats, R.S., 1998, Structure and shortening of the Kangra and Dehra Dun reentrants, Sub-Himalaya, India: *Geological Society of America Bulletin*, v. 110, no. 8, p. 1010–1027, [https://doi.org/10.1130/0016-7606\(1998\)110<1010:SASOTK>2.3.CO;2](https://doi.org/10.1130/0016-7606(1998)110<1010:SASOTK>2.3.CO;2).
- Robert, X., Van der Beek, P., Braun, J., Perry, C., and Mugnier, J.-L., 2011, Control of detachment geometry on lateral variations in exhumation rates in the Himalaya: Insights from low-temperature thermochronology and numerical modeling: *Journal of Geophysical Research. Solid Earth*, v. 116, B05202, <https://doi.org/10.1029/2010JB007893>.
- Robinson, D.M., DeCelles, P.G., Garzzone, C.N., Pearson, O.N., Harrison, T.M., and Catlos, E.J., 2003, Kinematic model for the Main Central Thrust in Nepal: *Geology*, v. 31, p. 359–362, [https://doi.org/10.1130/0091-7613\(2003\)031<0359:KMFTMC>2.0.CO;2](https://doi.org/10.1130/0091-7613(2003)031<0359:KMFTMC>2.0.CO;2).
- Robl, J., Stüwe, K., Hergarten, S., 2008, Channel profiles around Himalayan river anticlines: Constraints on their formation from digital elevation model analysis: *Tectonics*, v. 27, TC3010, <https://doi.org/10.1029/2007TC002215>.
- Robl, J., Hergarten, S., and Prasicek, G., 2017, The topographic state of fluvially conditioned mountain ranges: *Earth-Science Reviews*, v. 168, p. 190–217, <https://doi.org/10.1016/j.earscirev.2017.03.007>.
- Schelling, D., and Arita, K., 1991, Thrust tectonics, crustal shortening, and the structure of the far-eastern Nepal Himalaya: *Tectonics*, v. 10, no. 5, p. 851–862, <https://doi.org/10.1029/91TC01011>.
- Scherler, D., Bookhagen, B., and Strecker, M.R., 2014, Tectonic control on <sup>10</sup>Be-derived erosion rates in the Garhwal Himalaya, India: *Journal of Geophysical Research, Earth Surface*, v. 119, no. 2, p. 83–105, <https://doi.org/10.1002/2013JF002955>.
- Scherler, D., Bookhagen, B., Wulf, H., Preusser, F., and Strecker, M.R., 2015, Increased late Pleistocene erosion rates during fluvial aggradation in the Garhwal Himalaya, northern India: *Earth and Planetary Science Letters*, v. 428, p. 255–266, <https://doi.org/10.1016/j.epsl.2015.06.034>.

- Scherler, D., DiBiase, R.A., Fisher, G.B., and Avouac, J.-P., 2017, Testing monsoonal controls on bedrock river incision in the Himalaya and Eastern Tibet with a stochastic-threshold stream power model: *Journal of Geophysical Research, Earth Surface*, v. 122, p. 1389–1429, <https://doi.org/10.1002/2016JF004011>.
- Schwanghart, W., and Scherler, D., 2014, Short Communication: TopoToolbox 2—MATLAB-based software for topographic analysis and modeling in Earth surface sciences: *Earth Surface Dynamics*, v. 2, no. 1, p. 1–7, <https://doi.org/10.5194/esurf-2-1-2014>.
- Seeber, L., and Armbruster, J.G., 1981, Great detachment earthquakes along the Himalayan Arc and long-term forecasting, in Simpson, D.W., and Richards, P.G., eds., *Earthquake Prediction: An International Review*: Washington, DC, American Geophysical Union, <https://doi.org/10.1029/ME004p0259>.
- Seeber, L., and Gornitz, V., 1983, River profiles along the Himalayan Arc as indicators of active tectonics: *Tectonophysics*, v. 92, p. 335–367, [https://doi.org/10.1016/0040-1951\(83\)90201-9](https://doi.org/10.1016/0040-1951(83)90201-9).
- Steck, A., 2003, Geology of the NW Indian Himalaya: *Eclogae Geologicae Helveticae*, v. 96, p. 147–196.
- Stevens, V.L., and Avouac, J.P., 2015, Interseismic coupling on the main Himalayan thrust: *Geophysical Research Letters*, v. 42, no. 14, p. 5828–5837, <https://doi.org/10.1002/2015GL064845>.
- Stübner, K., Grujic, D., Dunkl, I., Thiede, R., and Eugster, P., 2018, Pliocene episodic exhumation and the significance of the Munsiri thrust in the northwestern Himalaya: *Earth and Planetary Science Letters*, v. 481, p. 273–283, <https://doi.org/10.1016/j.epsl.2017.10.036>.
- Stüwe, K., Robl, J., Hergarten, S., and Evans, L., 2008, Modeling the influence of horizontal advection, deformation, and late uplift on the drainage development in the India–Asia collision zone: *Tectonics*, v. 27, no. 6, <https://doi.org/10.1029/2007TC002186>.
- Thakur, V.C., Pandey, A.K., and Suresh, N., 2007, Late Quaternary–Holocene evolution of dun structure and the Himalayan Frontal Fault zone of the Garhwal Sub-Himalaya, NW India: *Journal of Asian Earth Sciences*, v. 29, no. 2–3, p. 305–319, <https://doi.org/10.1016/j.jseas.2006.02.002>.
- Thakur, V.C., Jayagondaperumal, R., and Malik, M.A., 2010, Redefining Medlicott–Wadia's main boundary fault from Jhelum to Yamuna: An active fault strand of the main boundary thrust in northwest Himalaya: *Tectonophysics*, v. 489, no. 1–4, p. 29–42, <https://doi.org/10.1016/j.tecto.2010.03.014>.
- Thakur, V.C., Joshi, M., Sahoo, D., Suresh, N., Jayagondaperumal, R., and Singh, A., 2014, Partitioning of convergence in Northwest Sub-Himalaya: Estimation of late Quaternary uplift and convergence rates across the Kangra reentrant, North India: *International Journal of Earth Sciences*, v. 103, no. 4, p. 1037–1056, <https://doi.org/10.1007/s00531-014-1016-7>.
- Thiede, R.C., and Ehlers, T.A., 2013, Large spatial and temporal variations in Himalayan denudation: *Earth and Planetary Science Letters*, v. 371–372, p. 278–293, <https://doi.org/10.1016/j.epsl.2013.03.004>.
- Thiede, R.C., Ehlers, T.A., Bookhagen, B., and Strecker, M.R., 2009, Erosional variability along the northwest Himalaya: *Journal of Geophysical Research*, v. 114, <https://doi.org/10.1029/2008JF001010>.
- Thiede, R., Robert, X., Stübner, K., Dey, S., and Faruhn, J., 2017, Sustained out-of-sequence shortening along a tectonically active segment of the Main Boundary thrust: The Dhauladhar Range in the northwestern Himalaya: *Lithosphere*, v. 9, no. 5, p. 715–725, <https://doi.org/10.1130/L630.1>.
- Thöni, M., Miller, C., Hager, C., Grasemann, B., and Horschinegg, M., 2012, New geochronological constraints on the thermal and exhumation history of the Lesser and Higher Himalayan Crystalline units in the Kullu–Kinnaur area of Himachal Pradesh (India): *Journal of Asian Earth Sciences*, v. 52, p. 98–116, <https://doi.org/10.1016/j.jseas.2012.02.015>.
- Van der Beek, P., Litty, C., Baudin, M., Mercier, J., Robert, X., and Hardwick, E., 2016, Contrasting tectonically driven exhumation and incision patterns, western versus central Nepal Himalaya: *Geology*, v. 44, p. 327–330, <https://doi.org/10.1130/G37579.1>.
- Vannay, J.-C., Grasemann, B., Rahn, M., Frank, W., Carter, A., Baudraz, V., and Cosca, M., 2004, Miocene to Holocene exhumation of metamorphic crustal wedges in the NW Himalaya: Evidence for tectonic extrusion coupled to fluvial erosion: *Tectonics*, v. 23, <https://doi.org/10.1029/2002TC001429>.
- Wang, Q., Zhang, P.Z., Freymueller, J.T., Bilham, R., Larson, K.M., and Lai, X., 2001, Present-day crustal deformation in China constrained by global positioning system measurements: *Science*, v. 294, no. 5542, p. 574–577, <https://doi.org/10.1126/science.1063647>.
- Wesnously, S.G., Kumar, S., Mohindra, R., and Thakur, V.C., 1999, Uplift and convergence along the Himalayan Frontal Thrust of India: *Tectonics*, v. 18, no. 6, p. 967–976, <https://doi.org/10.1029/1999TC900026>.
- Whipple, K.X., and Tucker, G.E., 1999, Dynamics of the stream-power river incision model: Implications for height limits of mountain ranges, landscape response timescales, and research needs: *Journal of Geophysical Research*, v. 104, B8, p. 17661–17674, <https://doi.org/10.1029/1999JB900120>.
- Whipple, K.X., Shirzaei, M., Hodges, K.V., and Arrowsmith, R.J., 2016, Active shortening within the Himalayan orogenic wedge implied by the 2015 Gorkha earthquake: *Nature Geoscience*, v. 9, p. 711–716, <https://doi.org/10.1038/ngeo2797>.
- Wobus, C.W., Hodges, K.V., and Whipple, K.X., 2003, Has focused denudation sustained active thrusting at the Himalayan topographic front?: *Geology*, v. 31, p. 861–864, <https://doi.org/10.1130/G19730.1>.
- Wobus, C.W., Whipple, K.X., and Hodges, K.V., 2006a, Neotectonics of the central Nepalese Himalaya: Constraints from geomorphology, detrital  $^{40}\text{Ar}/^{39}\text{Ar}$  thermochronology, and thermal modeling: *Tectonics*, v. 25, <https://doi.org/10.1029/2005TC001935>.
- Wobus, C.W., Whipple, K.X., Kirby, E., Snyder, N., Johnson, J., and Spyropoulos, K., Crosby, B., and Sheehan, D., 2006b, Tectonics from topography: Procedures, promise, and pitfalls, in Willett, S.D., Hovius, N., Brandon, M.T., Fisher, D.M., eds., *Tectonics, Climate, and Landscape Evolution: Geological Society of America Special Paper 398*, p. 55–74, [https://doi.org/10.1130/2006.2398\(04\)](https://doi.org/10.1130/2006.2398(04)).
- Wulf, H., Bookhagen, B., and Scherler, D., 2010, Seasonal precipitation gradients and their impact on fluvial sediment flux in the Northwest Himalaya: *Geomorphology*, v. 118, no. 1–2, p. 13–21, <https://doi.org/10.1016/j.geomorph.2009.12.003>.
- Yeats, R.S., and Lillie, R.J., 1991, Contemporary tectonics of the Himalayan frontal fault system: Folds, blind thrusts, and the 1905 Kangra earthquake: *Journal of Structural Geology*, v. 13, p. 215–225, [https://doi.org/10.1016/0191-8141\(91\)90068-T](https://doi.org/10.1016/0191-8141(91)90068-T).
- Yin, A., 2006, Cenozoic tectonic evolution of the Himalayan orogen as constrained by along-strike variation of structural geometry, exhumation history, and foreland sedimentation: *Earth-Science Reviews*, v. 76, no. 1–2, p. 1–131, <https://doi.org/10.1016/j.earscirev.2005.05.004>.

MANUSCRIPT RECEIVED 8 JUNE 2017

REVISED MANUSCRIPT RECEIVED 30 APRIL 2018

MANUSCRIPT ACCEPTED 4 JUNE 2018